

UC San Diego

UC San Diego Previously Published Works

Title

Frontogenesis and the Creation of Fine-Scale Vertical Phytoplankton Structure

Permalink

<https://escholarship.org/uc/item/89d5z75q>

Journal

Journal of Geophysical Research - Oceans, 124(3)

ISSN

2169-9275

Authors

Verneil, A
Franks, PJS
Ohman, MD

Publication Date

2019-03-01

DOI

10.1029/2018jc014645

Peer reviewed

Frontogenesis and the Creation of Fine-Scale Vertical Phytoplankton Structure

A. de Verneil¹ , P. J. S. Franks² , and M. D. Ohman² 

¹The Center for Prototype Climate Modeling, New York University Abu Dhabi, Abu Dhabi, United Arab Emirates,

²Scripps Institution of Oceanography, University of California, San Diego, La Jolla, CA, USA

Key Points:

- Observations show biological gradients downstream of frontogenesis collocated with FSLE structures
- Phytoplankton patch orientations are consistent with frontal ageostrophic secondary circulation
- Frontal phytoplankton patch reorientation could impact exposure to light and zooplankton grazing

Supporting Information:

- Supporting Information S1
- Figure S1
- Figure S2
- Figure S3
- Figure S4

Correspondence to:

A. de Verneil,
ajdl11@nyu.edu

Citation:

de Verneil, A., Franks, P. J. S., & Ohman, M. D. (2019). Frontogenesis and the creation of fine-scale vertical phytoplankton structure. *Journal of Geophysical Research: Oceans*, 124. <https://doi.org/10.1029/2018JC014645>

Received 9 OCT 2018

Accepted 3 FEB 2019

Accepted article online 6 FEB 2019

Abstract Fine-scale spatial structuring of phytoplankton patches has significant consequences for the marine food web, from altering phytoplankton exposure to surface light and limiting nutrients, to influencing the foraging of zooplankton, modifying carbon export, and impacting patterns of diversity. Hence, it is important to identify these fine-scale features and determine what generates their variability. Here we present evidence of fine-scale, tilted, interleaved layers in salinity and chlorophyll-*a* fluorescence observed in free-fall Moving Vessel Profiler surveys across a frontal system west of Point Conception, California. The observed covariability of hydrographic and biological properties allows for decomposition of the features into different water histories. Our analyses suggest that recently upwelled coastal water subsequently advected and intermingled with surrounding water masses from farther offshore. Orientations of the fine layers found in the filament are consistent with restratification and downwelling due to an ageostrophic secondary circulation brought on by frontogenesis. Finite size Lyapunov exponents, a Lagrangian diagnostic calculated from remote sensing data, provide positive evidence for frontogenetic convergence occurring upstream of the feature and allow for direct comparisons with in situ data to gauge their general utility in defining dynamical boundaries. These results highlight how frontal systems not only horizontally compress the biological niches represented by formerly disparate water masses but also create vertical structure and patchiness that can rapidly change over submesoscales.

Plain Language Summary Like weather in the atmosphere, frontal systems form in the ocean at the boundary of two different bodies of water. Phytoplankton, the organisms at the base of the marine food web, can find themselves brought into fronts by surface currents. When this happens, patches of phytoplankton are stretched along the front. The circulation at these fronts also causes the patches to tilt across the front, leading to stacked layers which we observed from a ship in the waters off California. When this happens, it changes how much light they receive for photosynthesis and how much of a target they are for the zooplankton that eat them. Besides taking up the greenhouse gas CO₂, phytoplankton growth ultimately determines how much food is available for commercial fish to eat. Therefore, the layering process we describe shows how frontal currents can impact the functioning of the marine food web.

1. Introduction

Phytoplankton in the surface ocean are often found in patchy distributions. Plankton patches can be characterized by their vertical or horizontal extent and can be expressed on multiple spatial scales. In the present study, we focus on patches of 1- to 10-m vertical and 10-m to 10-km horizontal extent, respectively. The mechanisms generating the formation of these patches include cell buoyancy, behavioral patterns, grazing, or advection (see Guasto et al., 2012, for a review of vertical patch formation, and Martin, 2003, for horizontal patches). Patchiness in plankton can reflect gradients of both biomass and diversity. The location of these gradients in the water column can profoundly affect not only the phytoplankton themselves, through access to surface light for photosynthesis and limiting nutrients found at depth (or supplied horizontally), but the foraging efficiency of their grazers (Cowles et al., 1998; Powell & Ohman, 2015). Therefore, the localization of patches, and the mechanisms generating their structure, has direct impacts upon local trophic exchanges.

Surface ocean fronts are regions of enhanced physical gradients that often coincide with biological transitions. Studies of phytoplankton at fronts often focus on ecosystem responses to bottom-up control by vertical nutrient and biomass fluxes at fronts (Lévy et al., 2001; Li et al., 2012; Nagai et al., 2008; Oguz et al., 2014; Spall & Richards, 2000; Strass, 1992; Zakardjian & Prieur, 1998). In addition to the vertical movement of

water, the currents at fronts also structure horizontal patchiness. For example, a strong horizontal density gradient and its associated geostrophic current can act as a barrier to cross-front dispersal, maintaining diversity at mesoscales (10–100 km) within enclosed eddy vortices (d'Ovidio et al., 2010). Additionally, the along-front vertical shear of a geostrophic frontal current has been shown to create thin layers inside and oriented along the front (Johnston et al., 2009). Thus, within a frontal feature there are many mechanisms that can affect the placement, structure, and dynamics of plankton patches.

Plankton patches observed in fronts can also reflect processes that occurred upstream of the front. The physical flows at a front are governed by the front's density structure and forcing. While salinity and temperature both contribute to density, they can do so in a compensatory fashion, resulting in a uniform density with different hydrographic characteristics. Essentially, these density-compensated gradients in salinity and temperature are negligible for most dynamical considerations at a front (though also see Similar comment as above re: semicolon. Hosegood et al., 2006). Density compensation has been widely observed in the ocean (Arhan, 1990; Roden, 1977; Yuan & Talley, 1992), and compensated gradients in salinity and temperature can persist for longer time scales than equivalent gradients in density before diffusing (Chin & Young, 1995). For example, compensated gradients will persist beyond the time scales of baroclinic instability (weeks–months; Tulloch et al., 2011) or days to weeks for submesoscale motions (Boccaletti et al., 2007). Because phytoplankton gradients do not impact physical flows in a significant way, large-scale gradients can be deformed into smaller-scale patches along isopycnals, including the submesoscale (Ferrari & Rudnick, 2000; Klein et al., 1998). The mechanism for generating compensated gradients is mesoscale stirring (Smith & Ferrari, 2009); fine-scale density-compensated layers in salinity have been observed by shipboard surveys in the northeastern Pacific (Shcherbina et al., 2010) and glider surveys in the Peru-Chile Upwelling region (Pietri et al., 2013) in association with mesoscale features.

In this study, we present observational evidence of small-scale vertical and horizontal variability in two tracers across a front in the California Current: salinity and chlorophyll-*a* (Chl-*a*) fluorescence. While the observation of small-scale variability in itself is not novel, this data set provides a unique opportunity. The data are located in a front that underwent recent frontogenesis, or strengthening of a frontal gradient. Beyond creating horizontal gradients by bringing distant water masses together, the data set demonstrates how frontogenesis also creates vertical gradients through restratification. The features we analyze here have been shown to be sites of enhanced vertical carbon export (Stukel et al., 2017) and a region of strong gradients of shell dissolution of shell-bearing pteropods (Bednaršek & Ohman, 2015). The rest of the paper is structured as follows: section 2 describes the observational context, collection procedure, and treatment methodology for the data used in this study. Section 3 presents our results, including the spatial distribution of the tracers and the identification of pertinent features for later discussion of the relevant dynamics in section 4. We conclude this study in section 5 with speculation regarding the general role the observed physical circulation may have upon phytoplankton patchiness at fronts.

2. Materials and Methods

2.1. Cruise Sampling and Context

The data used in this study come from the 2012 process cruise (P1208), dubbed “E-Front,” of the NSF-funded California Current Ecosystem Long-Term Ecological Research program conducted from late July to late August aboard the R/V *Melville*. The cruise's main objectives were to identify regions of enhanced horizontal physical and biological gradients (i.e., fronts) and quantify their role in structuring the pelagic ecosystem and modifying carbon export. The study area was centered around a frontal structure observed off the coast of California, positioned roughly at 123°W and spanning 35.75° to 33°N (Figure 1). AVISO satellite sea surface height (SSH) data indicate the frontal region was roughly geostationary 1 month prior and subsequent to sampling (4 July and 4 September), existing at the boundary of an anticyclonic eddy to the west and a cyclonic eddy to the east. The SSH gradient resulted in geostrophic currents that flowed from north to south (Figure 1). A survey going north to south with the geostrophic jet was conducted with a free-fall Moving Vessel Profiler (MVP; Ohman et al., 2012). This survey produced four conductivity-temperature-depth (CTD) and Chl-*a* crossings of the frontal region over the course of 15 hr (Figures 1b and 1c). The MVP transects were followed by biological sampling and hydrographic surveys for the rest of the cruise, including overnight transects and multiday experimental cycles, similar to Landry et al. (2009).

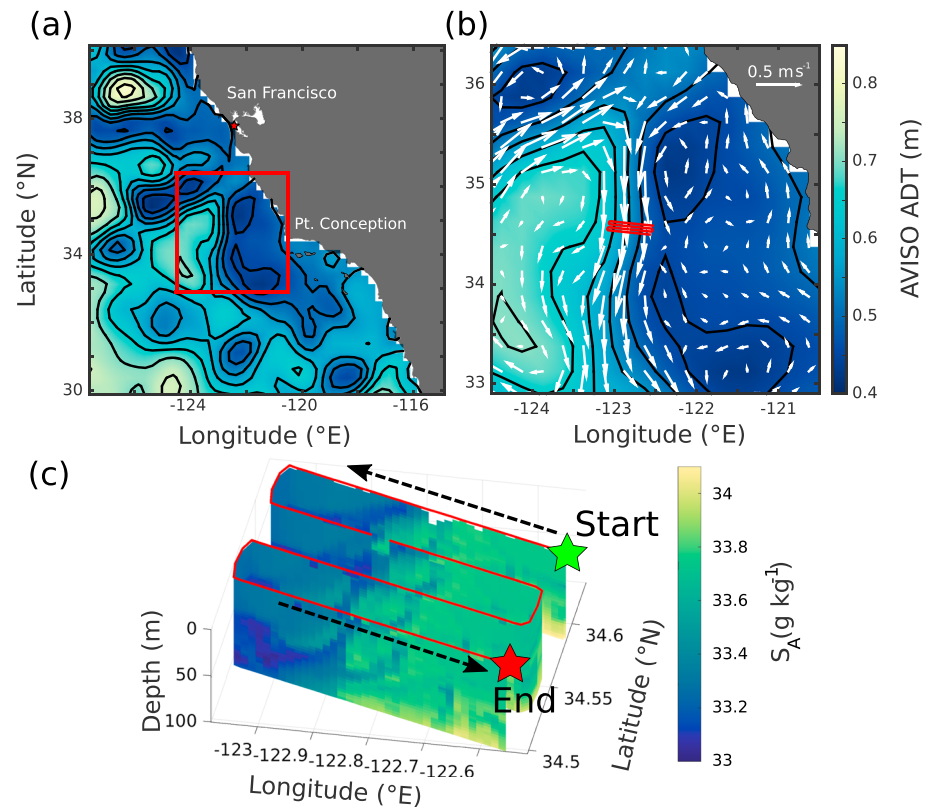


Figure 1. (a) Absolute dynamic topography (sea surface height) off the coast of California for 3 August 2012. Black contours are of sea surface height plotted every 5 cm, land shaded gray. Red box indicates area shown in (b). (b) Zoomed-in plot of topography, with similar color and shading to (a). White arrows show geostrophic currents associated with topography. Red lines show ship track during Moving Vessel Profiler transects. (c) Three-dimensional surface plot of absolute salinity S_A . Red line is the ship track, with green and red stars marking the starting and ending positions, respectively.

2.2. MVP CTD Data

The majority of the data presented here derive from the MVP CTD surveys. Casts are on average 1.3 km apart, leading to four cross-front transects approximately 50 km in length and spaced 3.5 km apart. The MVP samples vertically by freewheeling the synthetic cable attached to the MVP fish, allowing for a near-vertical descent at ~ 4 m/s. At a prescribed depth (here set to 200 dBar), the brake is applied to the computer-controlled winch and the fish is automatically brought back to the surface. Only down-casts are used in this data set. On board the fish is a rapid-response AML Oceanographic μ conductivity sensor, thermometer, Chl-*a* fluorometer, and laser optical particle counter. The conductivity and temperature data were lag-corrected to reduce salinity spiking (supporting information Figure S1) before conversion to absolute salinity, S_A , conservative temperature, C_T , and potential density, ρ_θ , in accordance with the TEOS-10 standard (McDougall & Barker, 2011). A previous study utilizing MVP data found an operational threshold binning of ~ 1 m in the vertical (Li et al., 2012), but here we have chosen 3-m bins.

In vivo Chl-*a* fluorescence was calibrated to Chl-*a* extractions but not corrected for light-dependent nonphotochemical quenching (Müller et al., 2001). In the California Current Ecosystem region, light attenuation constants can be around 0.1 m^{-1} (Aksnes & Ohman, 2009), leading to light intensities at 30 m, where the Chl-*a* features highlighted in this study begin, that are $\leq 5\%$ of the surface value. Additionally, the 15 hr of the MVP survey began at 2:30 p.m. local time, with the high Chl-*a* features in the middle of the front being sampled after sunset (7:07 p.m.) for transects 2, 3, and 4. Therefore, Chl-*a* measurements were mostly taken after dark and we focus on depths far away from the surface to minimize the effect of nonphotochemical quenching. Notwithstanding the likely small effect of nonphotochemical quenching, this and other limitations prevent us from making quantitative comparisons among fluorescence patches in terms of phytoplankton biomass or population dynamics, a challenging problem (Kruskopf & Flynn, 2006). Consequently, for the

remainder of this study, fluorescence is used qualitatively to identify structure in the water column; we will focus solely on relative values.

Each transect is assumed to be synoptic. Averaging at 3.5 hr apiece, it is less than the inertial period of 21 hr, but higher-frequency phenomena such as internal waves are aliased. Density data are horizontally smoothed in order to remove these signals using a “locally weighted scatter plot smooth,” or “lowess,” polynomial fit spanning 10 observations, close to the observed along-transect decorrelation scale. Because tracer patchiness is the main focus of this study, the Chl-*a* and S_A data are not similarly smoothed. Instead, profiles are constructed by linearly interpolating density-tracer relationships from each initial profile onto the smoothed density profile to preserve density-tracer structure (Figure S2).

Satellite Chl-*a* and SST observations, which might serve as useful comparison to the in situ data, were not available during and the weeks before and during the sampling period due to cloud cover, though partial coverage is available for 12–19 August (Figure S3).

2.3. Finite Size Lyapunov Exponents

The mesoscale context for E-Front is evaluated using remote sensing data. Altimetry-derived geostrophic currents are provided by the delayed-time AVISO global gridded product with 0.25° resolution. The AVISO product has a daily resolution and can be downloaded at the Copernicus Marine Environment Monitoring Service website under data set “SEALEVEL_GLO_PHY_L4_REP_OBSERVATIONS_008_047” (marine.copernicus.eu). These currents are used to compute finite size Lyapunov exponents (FSLEs) using the algorithm of d’Ovidio et al. (2004). FSLEs are calculated by time-integrating particle trajectories with a fourth-order Runge-Kutta method with a 6-hr time step. Particles are initially separated by 0.01° and reach a final separation of 0.2° . Velocity fields are linearly interpolated in time and space. The integration is backward in time over a 30-day duration. As a result, the final separation represents the initial locations of particles that were subsequently brought together through convergent flows. A threshold value of 0.1 day^{-1} was imposed on the exponents. FSLE values often form continuous lines, or ridges, which are used to identify regions of enhanced strain that are to be expected near frontal zones or eddy edges. The ridges also indicate boundaries across which water exchange should be minimized and along which advection is maximized. By tracing ridges of FSLE backward from the survey region, they can be used to identify potential source regions for the water sampled during E-Front. FSLEs have been found in practice to serve as a useful heuristic for identifying flow manifolds in two-dimensional data, and the calculations are robust to small-scale errors in the velocity field (Cotté et al., 2011).

The relevance of FSLEs derived from 0.25° data to kilometer-scale in situ data derives from the theory of frontogenesis. During frontogenesis, an exponential compression of horizontal gradients occurs, leading to frontal dynamics. Idealized models of frontogenesis require a large-scale strain rate driven by mesoscale forcing (Hoskins, 1982). The FSLEs calculated by the satellite-derived advection field provide the locality and relative strength of the mesoscale forcing required to drive frontogenesis, which by its nature will produce gradients at small scales.

3. Results

As shown below, the MVP surveys crossed a strong density front in the survey region. The axis of the front was oriented north-south, with the surveys occurring about 200 km due west of Point Conception. Geostrophic currents at the front flowed south in a strong jet (Figure 1b). Cross-front transects (in this study figures of transects are oriented looking north) showed that the density front was characterized by distinct tongues of high-Chl-*a* and high-salinity water extending from the surface near the front down to 50- to 70-m depth, angling downward and westward (offshore) toward the less dense side of the front. The tongues were ~5–10 km in cross-front extent and appeared in all four transects. Here we explore the hydrographic and biological properties of these fine-scale features and use FSLE analysis to indicate potential geographic origins of their parent water masses.

3.1. Salinity and Chl-*a* Fluorescence Fine Structure

A density front was found in each of the four MVP transects (Figure 2). The $1,025\text{-kg/m}^3$ isopycnal outcrops or nearly outcrops at the surface in the center of the transects, extending upward from ~70-m depth offshore in the west, up toward the surface over ~25 km horizontally. This isopycnal then descends again to the

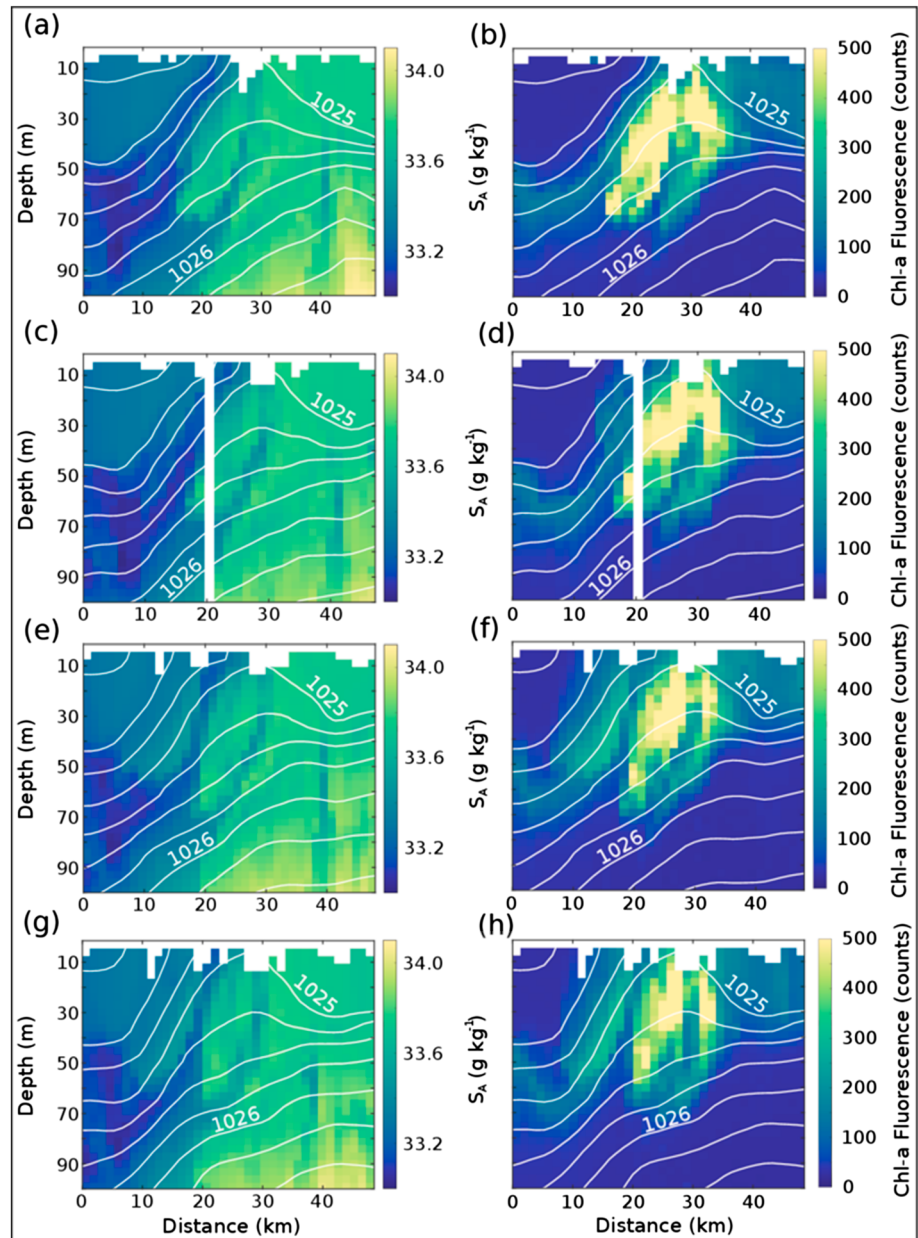


Figure 2. Absolute salinity, S_A (left column) and Chl-*a* (right column) for transects (a, b) 1, (c, d) 2, (e, f) 3, and (g, h) 4. Distance measured from westernmost position increasing eastward. Isopycnals shown in white, with contours drawn at every 0.25 kg/m^3 .

east, reaching $\sim 30\text{-m}$ depth over $\sim 20\text{-km}$ horizontal distance. The region where the $1,025\text{-kg/m}^3$ isopycnal appears closest to the surface is taken to be the center of the frontal zone. The doming of the $1,025\text{-kg/m}^3$ isopycnal in the center of the survey region is reminiscent of a cold-core filament; however, the deeper isopycnals rise in a mostly monotonic manner from west to east, indicating a “normal” front. As a result, the filament-like structure with a midtranssect density maximum appears to be confined above the $1,025.5\text{-kg/m}^3$ isopycnal.

The salinity and Chl-*a* distributions for the four transects show similar patterns around the density front (Figure 2). Overall, low-salinity, low-Chl-*a* water is found to the west of the front, and high-salinity, high-Chl-*a* waters occur to the east. A low-salinity layer around the $1,024.75\text{-}$ and $1,025\text{-kg/m}^3$ isopycnals on the west side of the front coincides with a weak, deep Chl-*a* maximum, while to the east of the front Chl-*a* maximal values are found in surface waters.

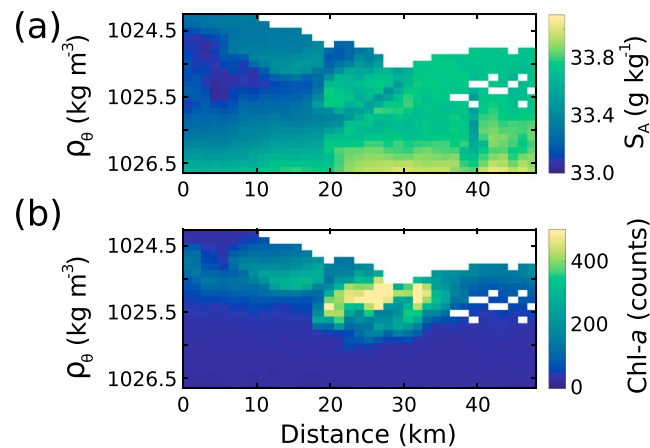


Figure 3. Transect 3 (a) S_A and (b) Chl- a in isopycnal coordinates.

At the frontal center Chl- a is considerably enhanced in two (transects 1 and 2; Figures 2b and 2d) or three (transects 3 and 4; Figures 2f and 2h) prominent tongues that extend from the surface at the front downward toward the west. These high-Chl- a tongues are about 5 km wide (across front), extending to 70 m below the surface, and are associated with similar tongues of relatively high salinity. The tongues of high salinity, high-Chl- a water are separated by layers of relatively low-salinity, low-Chl- a water with approximately the same dimensions as the high-salinity, high-Chl- a tongues. All tongues cross isopycnals, with the westernmost tongues (e.g., transects 3 and 4, Figures 2e–2h) crossing the 1024.75 and 1025 isopycnals, whereas the two easternmost tongues cross the 1025.25, 1025.5, and 1025.75 isopycnals.

The alternating layers found inside the front are sloped in the same direction as the isopycnals they are found in (downward toward the west). However, the layers' boundaries slope more sharply than the isopycnals, which can be confirmed by the residual slopes seen after transforming to isopycnal coordinates (Figure 3). Since the westernmost tongue traverses fewer isopycnals, its slope is less pronounced as the other tongues, indicating greater isopycnal alignment.

3.2. Salinity-Chl- a Fluorescence Distributions and T-S Context

On a salinity-Chl- a plot, S_A and Chl- a data produce a triangular distribution (Figure 4). At the salinity of 33.8 g/kg, a range of Chl- a values can be found, forming the right side of the triangle. Salinities as low as 33 g/kg are associated with low-Chl- a waters of the California Current. Low-Chl- a values can be found between the highest and lowest salinities, forming the bottom of the triangle. Joining the high-salinity, high-Chl- a waters and low-salinity, low-Chl- a waters is a side of the triangle representing covarying gradients in both salinity and Chl- a , presumably formed through mixing of the two end members.

Three salinity-Chl- a end members can be identified: 33.8 g/kg and 700 counts of S_A and Chl- a , respectively, represent waters from the middle of the front; 33.8 g/kg and 100 counts represent waters from the inshore side of the front; and 33.1 g/kg and 100 counts indicate offshore California Current waters. As a result, three water types have been demarcated, as follows:

1. High-Chl- a , high-salinity water (hereafter, HCHS-G; green), defined as observations with Chl- a > 375 counts, resulting in S_A > 33.4 g/kg.
2. Low-Chl- a , low-salinity water (LCLS-B; blue), with $75 < \text{Chl-}a < 375$ counts, and $S_A < \text{line}$ defined by the points (33.4,75) and (33.6,375) in S_A -Chl- a space.
3. Low-Chl- a , high-salinity water (LCHS-R; red), with $75 < \text{Chl-}a < 375$, and $S_A > \text{line}$ defined by the points (33.6,75) and (33.65,375).

A temperature-salinity (T-S) plot reveals the relationships among these three water types (Figure 5). The HCHS-G and LCHS-R water, by virtue of their enhanced salinities and similar densities, cannot be separated from one another in their hydrographic properties. However, observations of LCHS-R water can be found at warmer temperatures than HCHS-G water, indicating surface heating. The HCHS-G and LCHS-R observations are embedded within the saltier, denser arm of the T-S plot representing the dense, inshore part of the front. LCLS-B water is found within the less salty arm of the T-S plots, forming the offshore part of the

front. The waters found with characteristics in between the two end-member arms of either side of the front are the HCHS-G and LCLS-B types.

3.3. FSLEs

Three separate FSLE ridges converge into the frontal zone sampled by the four MVP transects (Figure 6). All three ridges can be traced upstream nearly parallel to each other until 35.5°N. At this point, the two westernmost ridges veer west, into what we here identify as the offshore-source water mass. The eastern ridge, the strongest in magnitude, separates and continues farther north, making a final loop toward the coast. Given the strength and location of this FSLE ridge, this northern region appears to be the source of the waters forming the core of the front. Another FSLE ridge to the east does not enter the MVP survey area, reflecting instead the recirculation of the cyclonic mesoscale feature seen in SSH (Figure 1b). This region will be considered inshore relative to the other areas defined by the FSLE ridges that cross the survey region.

3.4. Water Type Distribution and FSLE Ridges

The water types identified through salinity-Chl-*a* relationships (Figure 4) are mapped, along with the advection pathways revealed by the FSLEs, onto their original spatial distributions in Figure 7. The strong, easternmost FSLE ridge is consistently found at or just to the east of where the 1,025-kg/m³ isopycnal shoals, demarcating the separation of frontal core water from inshore water. The middle FSLE ridge appears in the first transect (Figure 7a) west of the frontal core, between the 1,024.5- and 1,024.75-kg/m³ isopycnal outcrops and over a subsurface high-Chl-*a* tongue. This pattern repeats for the second transect (Figure 7b), while for the third and fourth transects this FSLE ridge is increasingly associated with the shoaling of the 1,025-kg/m³ isopycnal and the central Chl-*a* maximum (HCHS-G water; Figures 7c and 7d). The western FSLE ridge appears solidly in the offshore region, west of the salinity minimum layer for the first two transects (Figures 7a and 7b). In the third and fourth transects, however, the ridge is found over the 1,024.5-kg/m³ outcrop, associated with the westernmost Chl-*a* layer (LCLS-B water; Figures 2f and 2h). No 1,024.5-kg/m³ outcrops or surface-enhanced Chl-*a* values are found west of this FSLE ridge.

Below the surface it is clear that the various water masses identified by the salinity-Chl-*a* relationship (Figure 4) are associated with distinct parts of the frontal distribution, in particular, the tongues of high

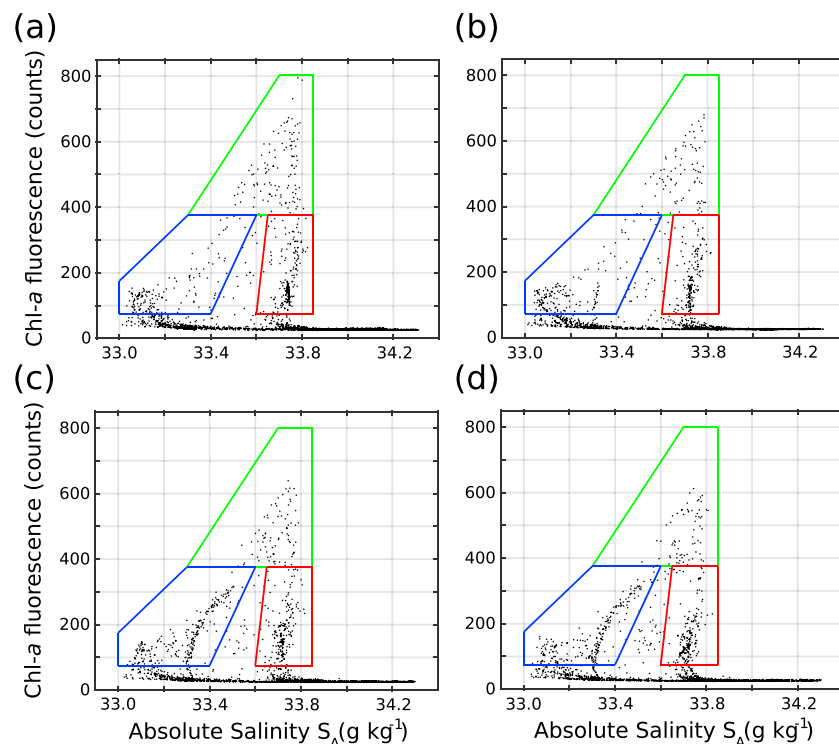


Figure 4. Chl-*a* and S_A distributions for transects 1–4 (a–d). Black dots indicate binned observations. Green box designates “high-Chl-*a*, high-salinity” water, blue box designates “low-Chl-*a*, low-salinity” water, and red box shows “low-Chl-*a*, high-salinity” water.

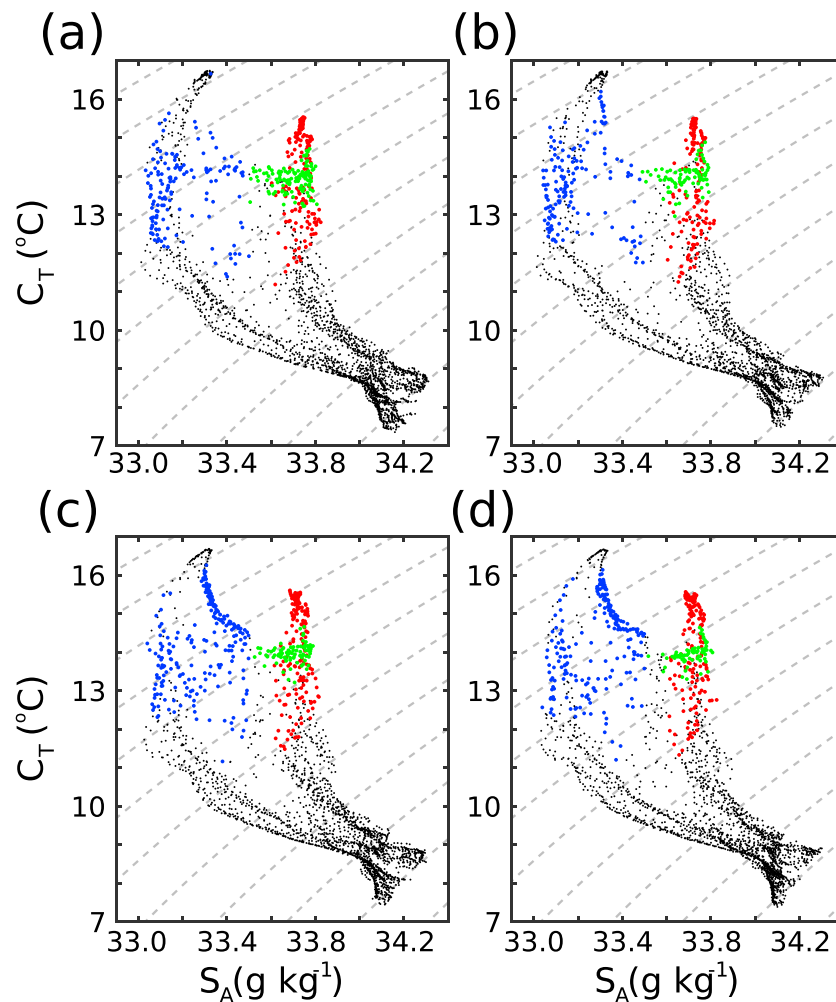


Figure 5. T-S diagrams for transects 1–4 (a–d). Gray contours are isopycnals, and black dots are observations not categorized by the salinity–Chl-*a* relationships. Green dots indicate high-Chl-*a*, high-salinity water. Red dots show low-Chl-*a*, high-salinity water. Blue dots represent low-Chl-*a*, low-salinity water.

Chl-*a*. The westernmost high Chl-*a* tongue—most apparent in transects 3 and 4 (Figures 7c and 7d) and mostly LCLS-B water—has lower salinities and is associated with offshore, California Current waters. This tongue lies under the western ridge of FSLE that can be traced back to the north of the survey area, turning abruptly westward at $\sim 35.5^\circ N$. Advection along this FSLE ridge would indicate source waters to the north and west of the frontal system.

The easternmost high-Chl-*a* tongue is associated with saltier waters of HCHS-G and LCHS-R types ($33.8\ g/kg$) and the strong eastern ridge of FSLE. The highest Chl-*a* values are found at about 20-m depth, although a distinct Chl-*a* tongue extends down to $\sim 70\ m$, where observations begin to be classified as LCHS-R. The FSLE ridge associated with this easternmost tongue of high-Chl-*a* water originates north and slightly east of the frontal region, near the coastal upwelling region (Figure 6b).

The water-type categorization reveals that the middle high-Chl-*a* tongue is mostly HCHS-G water, both salty and enhanced in Chl-*a*. This tongue extends down to 70 m, angling westward with depth. At the surface, it lies to the east or slightly under the middle ridge of FSLE, which originates northward and offshore (Figure 6b). At depth and in between the tongues, layers of fresher water with low Chl-*a* can be found. For all transects, most of the observations between the central and eastern Chl-*a* tongues indicate LCHS-R waters. However, there are at least a few observations of LCLS-B water as well. For transects 3 and 4, where the western Chl-*a* tongue is present, another layer is formed between this tongue and the HCHS-G central tongue.

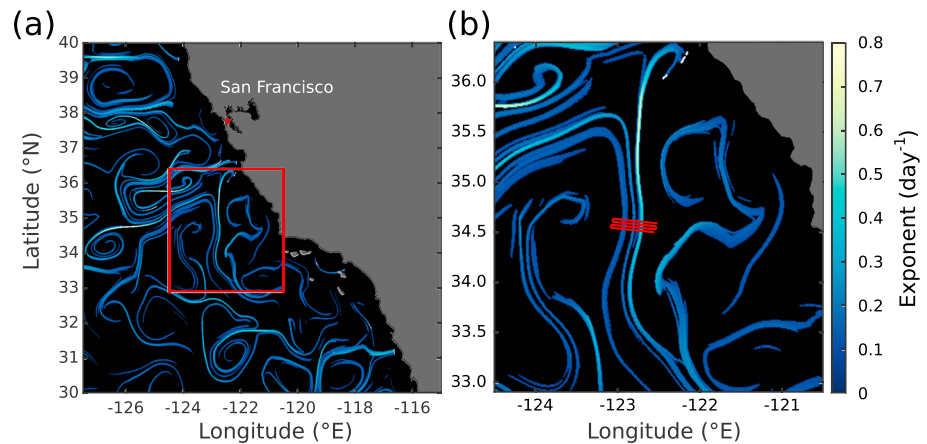


Figure 6. (a) FSLEs off the coast of California for 4 August 2012. Red box and shading similar to Figure 1. (b) Zoomed-in view of FSLEs, with red lines showing ship track during Moving Vessel Profiler transects as in Figure 1b. FSLE = finite size Lyapunov exponent.

The majority of observations in this region are LCLS-B, with few observations of LCHS-R water found at depth.

4. Discussion

Closely spaced CTD-fluorescence transects across a density front in the California Current System showed isolated tongues of relatively high salinity and high Chl-*a* extending downward from the surface of the front. Analyses of the hydrographic and biological properties of these tongues, combined with FSLEs calculated from remotely sensed SSH, suggest that the tongues had geographically distinct origins and were brought together by the mesoscale convergence of disparate water masses at the front.

By their nature as lines indicating advective barriers, the FSLEs give a Lagrangian trail by which the water masses observed in the MVP surveys can be traced back to their sources. Three notable ridges of FSLE could be identified in the cross-front MVP survey region: two ridges with offshore (western) provenance and one from a northerly coastal origin. These three ridges—and their associated water masses—converged together north of the MVP surveys near 35.5°N (Figure 6). This convergence stretched water masses along the front and narrowed them across the front as they were brought into close (kilometer-scale) proximity. The FSLE ridges and the advective pathways they represent spanned the entire frontal region where isopycnals outcropped at the surface, suggesting that future sampling campaigns might use FSLEs to identify frontal zones and the water masses that compose them.

4.1. Formation of the Chl-*a* Tongues

The three tongues of high-Chl-*a* water observed at E-front were ~5–10 km wide across the front, separated by ~5-km-wide tongues of low-Chl-*a* water. Our analyses suggest that the westernmost and easternmost tongues had geographically distinct origins, coming from water masses >100 km apart: the western tongue associated with the offshore FSLE consisted of LCLS-B water with signatures of California Current waters. In contrast, the eastern tongue of HCHS-G and LCHS-R inshore water was associated with the FSLE originating from the coast. The central tongue, with a core of HCHS-G water, had inshore water properties but was associated with a western-source FSLE. The presence of LCLS-B and LCHS-R waters at the margins of the high Chl-*a* core further suggests that the two water masses were brought together around this central feature. Mesoscale convergence upstream of the front thus has the consequence of bringing disparate water masses initially separated by hundreds of kilometers together into a region only ~20 km wide (Figures S3 and S4).

The biological communities in these different water masses presumably had different origins and histories, presenting different community structures at kilometer scales across the front. The high salinities and colder temperatures of the eastern and central Chl-*a* tongues (HCHS-G water) indicate that it originated from upwelled water near the coast. The high nutrient concentrations in these source waters likely fueled enhanced new production, leading to the high Chl-*a* values in the HCHS-G waters. Further evidence of the water's recently upwelled nature is reflected in the fact that surface LCHS-R water is warmer than HCHS-G

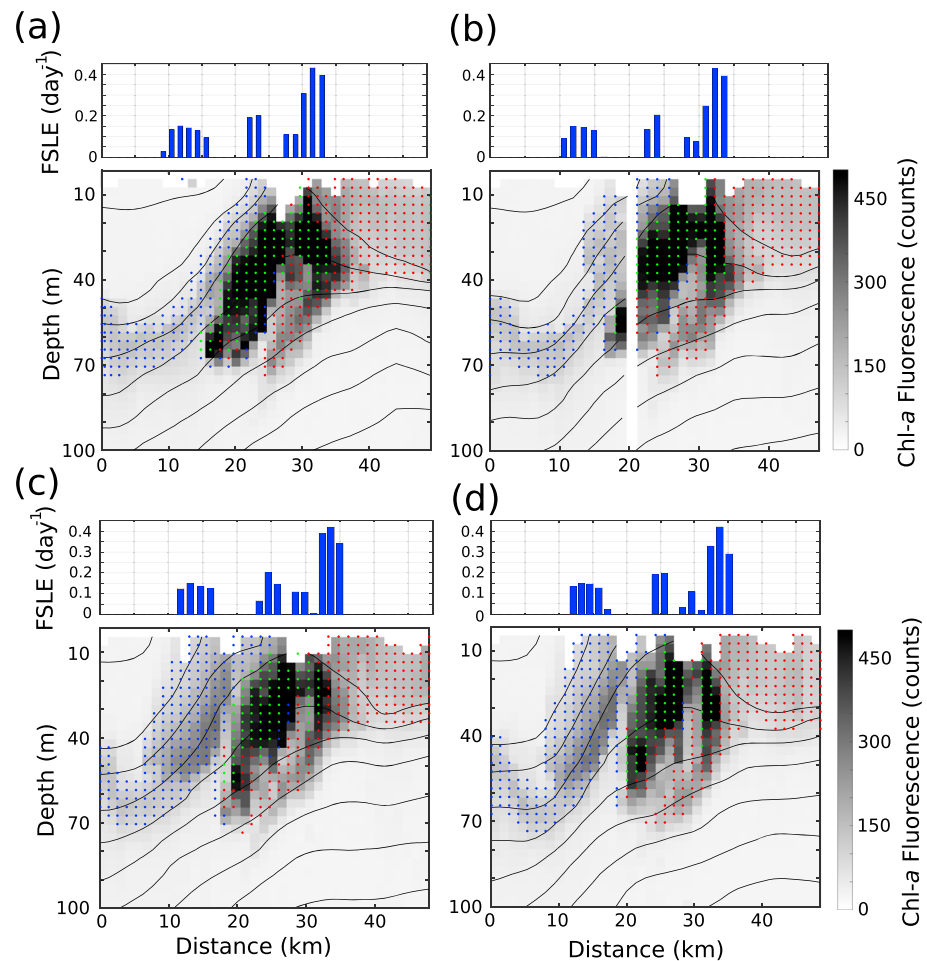


Figure 7. Water type distributions and FSLE values for transects 1–4 (a–d). Grayscale shading is Chl-*a* along with isopycnal contours, similar to Figure 3. Green, blue, and red dots indicate observations that fall within the water type designations shown in Figure 4. Top inset displays FSLE values along the transect. FSLE = finite size Lyapunov exponent.

water, because it has been exposed to surface heating for longer (Figure 5). The enhanced Chl-*a* in the westernmost tongue, with its offshore FSLE origin, could have developed in situ through nutrient fluxes (Li et al., 2012) in conjunction with the shoaling of the deep Chl-*a* maximum's layer. Additionally, mixing between LCLS-B and HCHS-G water may have played a role, further altering the biological community. The central tongue of high Chl-*a* at the frontal core and all three water types on its periphery represents a mixture of the coastal upwelled waters and waters of offshore origin, likely creating a patchy and diverse planktonic community there.

The vertical extent of the high Chl-*a* tongues at the front could come about via several different mechanisms, all of which could be operating simultaneously: (1) advection of source water properties, (2) response to local nutrient fluxes, and (3) intense upwelling/subduction of front waters.

First, the depth of the high Chl-*a* values could simply reflect the thickness of the layer in which this community was formed. The easternmost tongue, with its likely coastal upwelling origins, may have formed in a 30- to 50-m-thick surface layer at the coast (similar to the depths of enhanced Chl-*a* east of the front), which was subsequently advected and stretched along the front through mesoscale convergence. Second, the Chl-*a* in the westernmost tongue could have become enhanced through a growth response to upward nutrient fluxes at the less dense side of the front (Klein & Lapeyre, 2009), as mentioned previously. Third, the tongues may have been deepened by subduction. In regions of frontogenesis with enhanced strain, intensified vertical velocities are expected (Mahadevan & Tandon, 2006). Discerning between mechanism 1 and mechanisms 2 and 3 in the western and central/eastern tongues, respectively, would require upstream in situ data which

are not available. The three mechanisms considered here all reference physical forcing on the tongues. Biological mechanisms, such as particle sinking, do not explain the covariability of Chl-*a* with S_A which would be unaffected by such processes.

Beyond the mechanisms necessary for the generation of enhanced Chl-*a* patches and their vertical extent, the coherent alternating pattern of high and low values along multiple isopycnals rules out certain formation mechanisms. First, the alternating patches could not be the result of internal waves, as these signals were filtered out of our data a priori and gradients created by them would be the result of heaving isopycnals, which could not generate along-isopycnal gradients (Figure 3). Additionally, if diapycnal mixing was responsible for creating the tongues of enhanced (depleted) Chl-*a* water from above (below), their signature would be detectable by residual small-scale density gradients correlated with the alternating patches. While smoothing of horizontal density was used in the present analysis, the original unsmoothed data do not show such correlations (Figure S2). Therefore, the mechanism proposed by Nagai and Clayton (2017), where intrusive filaments of nitrate are attributed to near-inertial waves at a front coupled with mixing, is unlikely. Furthermore, while the water mass analysis suggests some mixing of HCHS-G and LCLS-B waters (Figure 5), *along-isopycnal* mixing would tend to erase gradients and patch structure, not create them. Instead, the features remain contiguous across multiple isopycnals. The most plausible mechanism to create the gradients observed involves the complicated merging of the multiple water masses at the front. Traditional models of frontogenesis employing equations such as quasi-geostrophy or semigeostrophy (Hoskins, 1982) invoke a single strain axis, whereas this front has multiple axes as suggested by the FSLEs. The dynamics resulting from a full, three-dimensional treatment of this front's forcing could lead to the nonintuitive intrusions seen, as in the results of Woods et al. (1986) using a primitive equation model for a meandering front (in particular, see their Figure 2). This mechanism becomes more plausible once the sharp turn of the offshore FSLEs, a form of meander, is considered (Figure 6). Given the diverse origins and history of the water masses at the front, in conjunction with the complicated frontogenetic forcing, it is unlikely that we will be able to definitively quantify the mechanisms leading to the precise origin and formation of these high Chl-*a* tongues at the front.

4.2. Tilting of the Chl-*a* Tongues

The tongues of high-Chl-*a* water observed at the front were consistently angled downward from east to west (Figures 2 and 3). Similar angled tongues of high-salinity water were recorded by Shcherbina et al. (2010) and Pietri et al. (2013) at fronts in the North and South Pacific, respectively. In both cases, the leading cause in creating the tracer patches was geostrophic turbulence (i.e., mesoscale stirring), whether due to a meandering front or local mesoscale eddies.

When fronts intensify during frontogenesis, meander, or are subject to certain wind and/or heating conditions, a rearrangement of water is needed to maintain thermal wind balance and conserve vorticity. The intensification of horizontal density gradients during frontogenesis accelerates geostrophic flow, with the tendency to destroy thermal wind balance (Hoskins, 1982). Balance is restored by vertical and cross-front velocities in what is called an ageostrophic secondary circulation (ASC) that has been known for decades (Eliassen, 1962; Sawyer, 1956). The immediate consequence is that water on the more (less) dense side of the front is subducted (upwelled), and surface (deep) cross-front velocities move toward the more (less) dense side of the front. In the present scenario, this would create a clockwise circulation when looking upstream of the front, resulting in vertical shear with surface currents moving east and deeper currents moving west. Naturally, any gradients or patches of phytoplankton embedded in this water would start to move with this flow and consequently deform to form layers (Franks, 1995).

The tracer slopes resulting from this and other forms of geostrophic turbulence has been predicted numerically to be $\sim f/N$ (f , Coriolis frequency and N , buoyancy frequency) and has been supported with observations from gliders (Smith & Ferrari, 2009; Cole & Rudnick, 2012). The f/N scaling largely reflects the aspect ratio between the vertical and horizontal velocities in the ASC. As a result, the tilting of the three Chl-*a* tongues was consistent with the direction of shear generated by an ASC during frontogenesis.

4.3. Vertical Fine Structure

Vertical profiles at the center of the front passed through several of the tongues of high and low Chl-*a* and salinity, giving a layered aspect to the profiles (Figure 8, positioned at 25.9-km distance in transect 3). Without the two-dimensional perspective provided by the MVP survey data, an individual profile would be difficult to interpret. Because patchiness is common in Chl-*a* profiles, it is not obvious that these layers

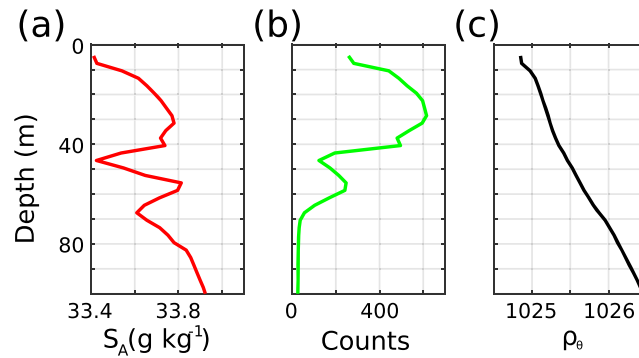


Figure 8. Vertical profiles of (a) S_A , (b) Chl-*a*, and (c) ρ_θ for cast 95 during transect 3.

might not reflect complex ecological variability but rather, as our analyses suggest, far-flung water masses vertically and horizontally juxtaposed during the course of mesoscale horizontal convergence and an ASC induced during frontogenesis. Thus, in active regions such as fronts, what might normally appear as local biological variability may actually reflect complicated flows combining different ecological communities.

4.4. A Conceptual Model for Layered Tongues at a Front

Though it is impossible to definitively assign specific dynamics to the formation of the high-Chl-*a* tongues seen in our cross-frontal surveys, our data suggest two dominant mechanisms: mesoscale stirring/forcing and ageostrophic cross-frontal circulation. Curiously, neither of these processes is required (or likely) to have scales of variability as small as the scales of hydrographic and biological variability that they create.

Our conceptual model for the formation process begins with distinct water masses embedded in a convergent mesoscale flow (Figure 9a). At this point, horizontal variability has been already created or is ongoing, possibly by complex three-dimensional mesoscale stirring (Woods et al., 1986). As these water masses converge toward the front, they are compressed laterally across the front and stretched along it (Figures 9b and 9c). This process both brings previously separated water masses into close proximity and forms small-scale (submesoscale) cross-frontal features through the strain of the ambient mesoscale velocity field.

The convergence at the front will similarly compress and steepen isopycnals at the front, enhancing the cross-frontal density gradient, that is, frontogenesis (Figures 9d and 9e). To accommodate the enhanced density gradient, an ASC develops that tends to relax the isopycnals across the front and toward the horizontal (Figure 9e). This circulation eventually tilts the layers that were formed through convergence and horizon-

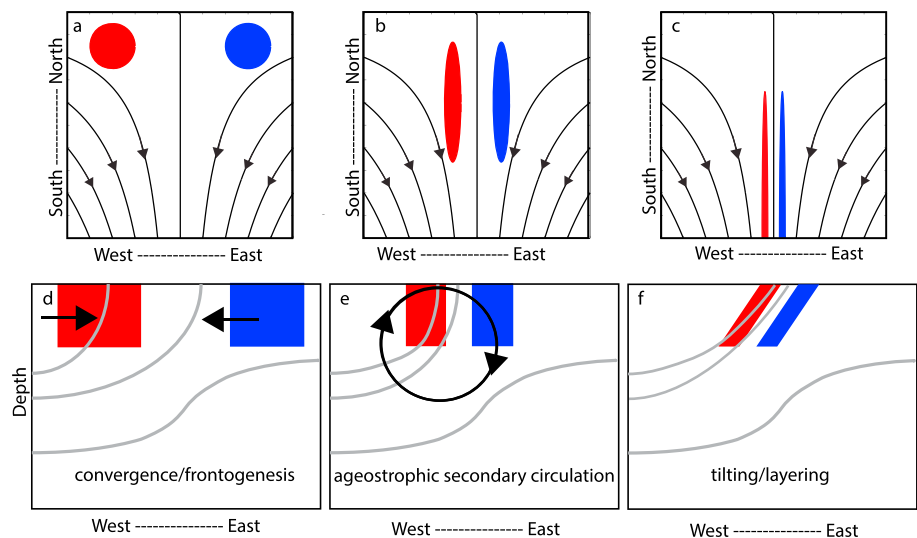


Figure 9. Idealized patch evolution during frontogenesis. (a–c) Top-down view of tracer patches (blue and red) in a convergent front, streamlines shown in black. (d–f) Side view of frontogenesis. Gray lines indicate isopycnals.

tal stirring (Figure 9f). Note that the ASC occurs at larger horizontal scales than the tongues formed through the horizontal convergence. Thus, the tongues were likely formed by the kinematics of horizontal stirring and convergence and tilted by a dynamic response of the front to convergence/frontogenesis.

Previous observations of layers, as well as the offshore export of near-shore material in the California Current, show similar results but do not combine the frontogenesis mechanism with small-scale variability. Shcherbina et al. (2010) showed thin layer variability resulting from forcing due to the meandering of a front in the North Pacific, and Pietri et al. (2013) found evidence of mesoscale stirring in the Peru-Chile upwelling system; these observations stem from the active strengthening of a front. The Coastal Transition Zone experiment (Brink & Cowles, 1991) conducted intensive surveys of upwelled water being exported offshore in a cold-core filament off the California Coast. Their findings of high phytoplankton activity (Hood et al., 1991), subduction (Kadko et al., 1991), and offshore transport in a filamental structure that can last a month (Chavez et al., 1991) are important findings that provide the context in which to interpret our data. Though the dynamics considered in the Coastal Transition Zone were similar to frontogenesis considered here, it is only with modern rapid sampling techniques that thin-layer vertical structures and their proper context are available in the present data set.

In sum, the combination of frontogenesis and its attendant ASC circulation cell not only sharpens preexisting horizontal gradients by compressing 100-km-scale variability into 10-km scales but then takes the structures at this smaller scale and rotates them to create new vertical gradients. These new vertical gradients can have important biological consequences for the growth of phytoplankton and the mesozooplankton that feed upon them.

5. Conclusions

In this study, we present observational evidence of fine-scale structure in Chl-*a* and S_A present inside a surface ocean front sampled off the coast of California during the upwelling season. The front was created between a cyclonic and anticyclonic circulation which induced frontogenesis. Inside the front, we find multiple tongues of water with enhanced Chl-*a* and salinity protruding from the surface and alternating with layers of fresher water and lower Chl-*a*. These layers are inclined in the same direction as the isopycnals sloping inside the front, but at steeper angles. FSLEs provide dynamical indicators showing where gradient tilting has occurred.

The exact scenario that initially created these alternating layers is likely complicated (Woods et al., 1986), and the spatial limitations of the data, and the three-dimensional nature of coastal upwelling, indicate that a coupled biological-physical modeling study would be useful to duplicate these observations. However, evidence that the layers originated upstream fulfills a precondition for demonstrating the effects of the circulation occurring within E-front. We suggest that the ASC created by frontogenesis, which restratifies density gradients, is a mechanism to tilt these layers through a vertical cross-frontal shear of horizontal velocities. While the shear due to thermal wind present inside fronts has been already implicated in creating thin layers *along* front (Johnston et al., 2009), this process creates layers across front. Due to the nature of frontogenesis in bringing different water masses into close proximity that then flow parallel along the front, strong horizontal biological gradients tend to exist preferentially across front rather than along front for frontal circulation to act upon. The tilting of enhanced Chl-*a* layers effectively spreads the distribution over a larger horizontal region while also thinning the layer, which can lead to enhanced light exposure due to the increased cross-sectional area and reduced self-shading. The increased cross section in turn can modify prey availability for vertically migrating grazers, and so both primary and secondary production can be influenced. These effects should be the focus of future in situ field campaigns to quantify their impact on the biological community in frontal regions.

References

- Aksnes, D. L., & Ohman, M. D. (2009). Multi-decadal shoaling of the euphotic zone in the southern sector of the California Current System. *Limnology and Oceanography*, 54(4), 1272–1281. <https://doi.org/10.4319/lo.2009.54.4.1272>
- Arhan, M. (1990). The North Atlantic current and subarctic intermediate water. *Journal of Marine Research*, 48(1), 109–144.
- Bednaršek, N., & Ohman, M. (2015). Changes in pteropod distributions and shell dissolution across a frontal system in the California Current System. *Marine Ecology Progress Series*, 523, 93–103. Retrieved from <https://www.int-res.com/abstracts/meps/v523/p93-103/>
- Boccaletti, G., Ferrari, R., & Fox-Kemper, B. (2007). Mixed layer instabilities and restratification. *Journal of Physical Oceanography*, 37(9), 2228–2250. <https://doi.org/10.1175/JPO3101.1>

Acknowledgments

We would like to thank Prof. Erick Fredj and one anonymous reviewer for their insights and comments that have produced a better paper. The altimeter products were produced by Ssalto/Duacs and distributed by Aviso+, with support from Cnes (<https://www.aviso.altimetry.fr/duacs/>). MVP data are publicly available within the CCE-LTER data system: <https://oceaninformatics.ucsd.edu/datazoo/catalogs/ccelter/datasets> and are being archived with the National Centers for Environmental Information (NCEI). We thank David Jensen for at-sea MVP visualization software, Michael Landry for his role as chief scientist, and the many participants in the CCE-LTER process cruise P1208 for their assistance in the field, including Chris Curl and the crew of the R/V *Melville*. We also thank Francesco d'Ovidio and Andrea Doglioli for FSLE software. Supported by NSF grants to the California Current Ecosystem LTER site.

- Brink, K. H., & Cowles, T. J. (1991). The Coastal Transition Zone program. *Journal of Geophysical Research*, 96(C8), 14,637–14,647. <https://doi.org/10.1029/91JC01206>
- Chavez, F. P., Barber, R. T., Kosro, P. M., Huyer, A., Ramp, S. R., Stanton, T. P., & Rojas de Mendiola, B. (1991). Horizontal transport and the distribution of nutrients in the Coastal Transition Zone off Northern California: Effects on primary production, phytoplankton biomass and species composition. *Journal of Geophysical Research*, 96(C8), 14,833–14,848. <https://doi.org/10.1029/91JC01163>
- Chin, L., & Young, W. (1995). Density compensated thermohaline gradients and diapycnal fluxes in the mixed layer. *Journal of Physical Oceanography*, 25(12), 3064–3075.
- Cole, S. T., & Rudnick, D. L. (2012). The spatial distribution and annual cycle of upper ocean thermohaline structure. *Journal of Geophysical Research*, 117, C02027. <https://doi.org/10.1029/2011JC007033>
- Cotté, C., d'Ovidio, F., Chaigneau, A., Lévy, M., Taupier-Letage, I., Mate, B., & Guinet, C. (2011). Scale-dependent interactions of Mediterranean whales with marine dynamics. *Limnology and Oceanography*, 56(1), 219–232.
- Cowles, T. J., Desiderio, R. A., & Carr, M. E. (1998). Small-scale planktonic structure: Persistence and trophic consequences. *Oceanography*, 11(1), 4–9. <http://www.jstor.org/stable/43924833>
- d'Ovidio, F., De Monte, S., Alvain, S., Dandonneau, Y., & Lévy, M. (2010). Fluid dynamical niches of phytoplankton types. *Proceedings of the National Academy of Sciences*, 107(43), 18,366–18,370.
- d'Ovidio, F., Fernández, V., Hernández-García, E., & López, C. (2004). Mixing structures in the Mediterranean Sea from finite-size Lyapunov exponents. *Geophysical Research Letters*, 31, 17. <https://doi.org/10.1029/2004GL020328>
- Eliassen, A. (1962). On the vertical circulation in frontal zones. *Geophys. Pub.*, 24(4), 147–160.
- Ferrari, R., & Rudnick, D. L. (2000). Thermohaline variability in the upper ocean. *Journal of Geophysical Research*, 105(C7), 16,857–16,883.
- Franks, P. J. (1995). Thin layers of phytoplankton: A model of formation by near-inertial wave shear. *Deep Sea Research Part I: Oceanographic Research Papers*, 42(1), 75–91. [https://doi.org/10.1016/0967-0637\(94\)00028-Q](https://doi.org/10.1016/0967-0637(94)00028-Q)
- Guasto, J. S., Rusconi, R., & Stocker, R. (2012). Fluid mechanics of planktonic microorganisms. *Annual Review of Fluid Mechanics*, 44, 373–400.
- Hood, R. R., Abbott, M. R., & Huyer, A. (1991). Phytoplankton and photosynthetic light response in the Coastal Transition Zone off Northern California in June 1987. *Journal of Geophysical Research*, 96(C8), 14,769–14,780. <https://doi.org/10.1029/91JC01208>
- Hosegood, P., Gregg, M. C., & Alford, M. H. (2006). Sub-mesoscale lateral density structure in the oceanic surface mixed layer. *Geophysical Research Letters*, 33, L22604. <https://doi.org/10.1029/2006GL026797>
- Hoskins, B. (1982). The mathematical theory of frontogenesis. *Review of Fluid Mechanics*, 14(1), 131–151.
- Johnston, T. S., Cheriton, O. M., Pennington, J. T., & Chavez, F. P. (2009). Thin phytoplankton layer formation at eddies, filaments, and fronts in a coastal upwelling zone. *Deep Sea Research Part II: Topical Studies in Oceanography*, 56(3-5), 246–259.
- Kadko, D. C., Washburn, L., & Jones, B. (1991). Evidence of subduction within cold filaments of the Northern California Coastal Transition Zone. *Journal of Geophysical Research*, 96(C8), 14,909–14,926. <https://doi.org/10.1029/91JC00885>
- Klein, P., & Lapeyre, G. (2009). The oceanic vertical pump induced by mesoscale and submesoscale turbulence. *Annual Review of Marine Science*, 1(1), 351–375. <https://doi.org/10.1146/annurev.marine.010908.163704>
- Klein, P., Treguier, A. M., & Hua, B. L. (1998). Three-dimensional stirring of thermohaline fronts. *Journal of Marine Research*, 56(3), 589–612.
- Kruskopf, M., & Flynn, K. J. (2006). Chlorophyll content and fluorescence responses cannot be used to gauge reliably phytoplankton biomass, nutrient status or growth rate. *New Phytologist*, 169(3), 525–536.
- Landry, M. R., Ohman, M. D., Goericke, R., Stukel, M. R., & Tsyrklevich, K. (2009). Lagrangian studies of phytoplankton growth and grazing relationships in a coastal upwelling ecosystem off Southern California. *Progress in Oceanography*, 83(1-4), 208–216.
- Lévy, M., Klein, P., & Treguier, A. M. (2001). Impact of sub-mesoscale physics on production and subduction of phytoplankton in an oligotrophic regime. *Journal of Marine Research*, 59(4), 535–565.
- Li, Q. P., Franks, P. J., Ohman, M. D., & Landry, M. R. (2012). Enhanced nitrate fluxes and biological processes at a frontal zone in the Southern California Current System. *Journal of Plankton Research*, 34(9), 790–801.
- Mahadevan, A., & Tandon, A. (2006). An analysis of mechanisms for submesoscale vertical motion at ocean fronts. *Ocean Modelling*, 14(3), 241–256. Retrieved from <http://www.sciencedirect.com/science/article/pii/S1463500306000540>. <https://doi.org/10.1016/j.ocemod.2006.05.006>
- Martin, A. (2003). Phytoplankton patchiness: The role of lateral stirring and mixing. *Progress in Oceanography*, 57(2), 125–174.
- McDougall, T. J., & Barker, P. M. (2011). Getting started with TEOS-10 and the Gibbs Seawater (GSW) oceanographic toolbox. *SCOR/IAPSO WG*, 127, 28.
- Müller, P., Li, X. P., & Niyogi, K. K. (2001). Non-photochemical quenching. A response to excess light energy. *Plant Physiology*, 125(4), 1558–1566.
- Nagai, T., & Clayton, S. (2017). Nutrient interleaving below the mixed layer of the Kuroshio Extension Front. *Ocean Dynamics*, 67(8), 1027–1046. <https://doi.org/10.1007/s10236-017-1070-3>
- Nagai, T., Tandon, A., Gruber, N., & McWilliams, J. C. (2008). Biological and physical impacts of ageostrophic frontal circulations driven by confluent flow and vertical mixing. *Dynamics of Atmospheres and Oceans*, 45(3-4), 229–251.
- Oguz, T., Macias, D., Garcia-Lafuente, J., Pascual, A., & Tintore, J. (2014). Fueling plankton production by a meandering frontal jet: A case study for the Alboran Sea (western Mediterranean). *PLoS One*, 9(11), e111482.
- Ohman, M. D., Powell, J. R., Picheral, M., & Jensen, D. W. (2012). Mesozooplankton and particulate matter responses to a deep-water frontal system in the Southern California Current System. *Journal of Plankton Research*, 34(9), 815–827.
- Pietri, A., Testor, P., Echevin, V., Chaigneau, A., Mortier, L., Eldin, G., & Grados, C. (2013). Finescale vertical structure of the upwelling system off southern Peru as observed from glider data. *Journal of Physical Oceanography*, 43(3), 631–646.
- Powell, J. R., & Ohman, M. D. (2015). Covariability of zooplankton gradients with glider-detected density fronts in the Southern California Current System. *Deep Sea Research Part II: Topical Studies in Oceanography*, 112, 79–90. Retrieved from <http://www.sciencedirect.com/science/article/pii/S0967064514001118> (CCE-LTER: Responses of the California Current Ecosystem to Climate Forcing). <https://doi.org/10.1016/j.dsr2.2014.04.002>
- Roden, G. I. (1977). Oceanic subarctic fronts of the central Pacific: Structure of and response to atmospheric forcing. *Journal of Physical Oceanography*, 7(6), 761–778.
- Sawyer, J. (1956). The vertical circulation at meteorological fronts and its relation to frontogenesis. *Proceedings of the Royal Society of London A: Mathematical, Physical and Engineering Sciences*, 234(1198), 346–362. Retrieved from <http://rspa.royalsocietypublishing.org/content/234/1198/346>. <https://doi.org/10.1098/rspa.1956.0039>
- Shcherbina, A., Gregg, M., Alford, M., & Harcourt, R. (2010). Three-dimensional structure and temporal evolution of submesoscale thermohaline intrusions in the North Pacific subtropical frontal zone. *Journal of Physical Oceanography*, 40(8), 1669–1689.

- Smith, K. S., & Ferrari, R. (2009). The production and dissipation of compensated thermohaline variance by mesoscale stirring. *Journal of Physical Oceanography*, *39*(10), 2477–2501.
- Spall, S., & Richards, K. (2000). A numerical model of mesoscale frontal instabilities and plankton dynamics—I. Model formulation and initial experiments. *Deep Sea Research Part I: Oceanographic Research Papers*, *47*(7), 1261–1301.
- Strass, V. H. (1992). Chlorophyll patchiness caused by mesoscale upwelling at fronts. *Deep Sea Research Part A: Oceanographic Research Papers*, *39*(1), 75–96.
- Stukel, M. R., Aluwihare, L. I., Barbeau, K. A., Chekalyuk, A. M., Goericke, R., Miller, A. J., & Landry, M. R. (2017). Mesoscale ocean fronts enhance carbon export due to gravitational sinking and subduction. *Proceedings of the National Academy of Sciences*, *114*(6), 1252–1257. Retrieved from <http://www.pnas.org/content/114/6/1252>. <https://doi.org/10.1073/pnas.1609435114>
- Tulloch, R., Marshall, J., Hill, C., & Smith, K. S. (2011). Scales, growth rates, and spectral fluxes of baroclinic instability in the ocean. *Journal of Physical Oceanography*, *41*(6), 1057–1076. <https://doi.org/10.1175/2011JPO4404.1>
- Woods, J., Onken, R., & Fischer, J. (1986). Thermohaline intrusions created isopycnally at oceanic fronts are inclined to isopycnals. *Nature*, *322*, 446–449. <https://doi.org/10.1038/322446a0>
- Yuan, X., & Talley, L. D. (1992). Shallow salinity minima in the North Pacific. *Journal of Physical Oceanography*, *22*(11), 1302–1316.
- Zakardjian, B., & Prieur, L. (1998). Biological and chemical signs of upward motions in permanent geostrophic fronts of the western Mediterranean. *Journal of Geophysical Research*, *103*(C12), 27,849–27,866.